ISSN: 2248-9622, Vol. 15, Issue 11, November 2025, pp 121-132

RESEARCH ARTICLE

OPEN ACCESS

Evaluation of the thermo-diffusion (Soret effect) impact across two phases of the alloys and the crystal-melt interface in In_{0.5}Ga_{0.5}Sb un-seeded crystallization growth by the VDS process

Dr Dattatray B. Gadkari¹

*Lead presenter: dr_gadkari@yahoo.com

1. Independent Researcher, Shree Yogesh Tower, Kora Kendra, Borivali (W), Mumbai 400092 India

ABSTRACT:

The high crystallization of $In_{0.5}Ga_{0.5}Sb$ under terrestrial gravity is severely affected by solutal convection and segregation, resulting in structural and compositional inhomogeneity. This study demonstrates an enhanced crystal-growth method using the Vertical Directional Solidification (VDS) process, where the crystal-melt interface is completely detached from the ampoule wall. The detachment minimizes lateral heat flux and suppresses convection, establishing a diffusion-dominated regime governed by thermodiffusion (Soret effect) and quasi-equilibrium kinetics. By optimizing the axial temperature gradient (12-28 °C cm⁻¹) and controlling the translation rate (< 3 mmh⁻¹), a stable planar interface was maintained throughout solidification. The resulting $1n_{0.5}Ga_{0.5}Sb$ crystals exhibit excellent structural perfection, high phase purity, and compositional uniformity ($\Delta x = -0.01$), These are confirmed by X-ray diffraction FWHM <100arcsec) and microstructural analyses. The interplay between complete detachment, thermal diffusion, and equilibrium control effectively replicates microgravity-like uniformity under Earth conditions. This reproducible and scalable approach provides a reliable pathway for growing high-quality detached crystals.

Keywords: VDS process; Directional solidification; Entire detached growth; Gradient freeze; Growth from melt; Antimonides; Semiconducting III–V material;

Date of Submission: 07-11-2025

Date of acceptance: 19-11-2025

I. Introduction:

Today's demand for the energy conversion

devices, and thermo-photovoltaic (TPV) cells is In₍₁₋ x)GaxSb (InGaSb) [1], but it is a challenge due to solidus-liquidus phases [2]. However, the partial detached growth in a space showed improved crystal, then, the moving meniscus model [6-15], and the solidification isotherm must below a meniscus [16-17] was proposed. The thermo-capillary model [18-19] and thermodynamic effect [20] for detached solidification were also proposed. GaSb:Te [21-22] growth in a space showed striation free, contactless growth, and InGaSb alloy thermal properties [23] were reported. But InGaSb growth [24] the steady state of equilibrium on Earth and a non-steady state of equilibrium in the melt composition with a higher growth rate was achieved in microgravity. The increased growth rate [25] and the enhanced homogeneous composition by heat and mass transfer by diffusion, crystals grow by the self-organization of atoms and molecules in a space and on Earth. GaSb:Te growth in a space and on Earth [26], the controlled thermo-solute velocity flow, heat and mass transfer by diffusion was achieved by eliminating thermo-gravitational convections.

In a space and on Earth, the numerical simulation (NS)of InGaSb [27-30], the axial temperature gradients, and cooling rate showed increased growth rate by diffusion, thus, the transformation of a melt phase to solid phase was successful. Whereas, NS-InGaSb growth by VGF [31-32] in microgravity, the phase transport phenomenon by an axial gradient, and cooling rates showed crystal uniformity, which was promoted flat interface front at low gradient, an ampoule rotation was studied. But on Earth [33], the concentration uniformity was achieved by minimized convection, whereas, in a space [34], showed higher growth rate and concave interface towards melt. The transport phenomena [35-36] of crystal growth by heat and mass transfer were reported. The temperature gradients (Soret effect) in isotropic vacuum sealed solute solution into ampoule creates an extraordinary medium, then convections can be neglected due to microgravity [35-38]. Numerical simulation of directional solidification process (NSSP) [39], the interaction between three solidified phases is a task.

The phase-field model [40] showed the melt cooled below the melting point grow the homogeneous seed. First time, the phase-field and rotating directional solidification (RDS) effect [41] was reported. In_{0.5}Ga_{0.5}Sb enhanced crystallization by an entire

detached growth, the transformation of melt phase to crystalline phase by controlled VDS configuration, the momentum at interface front grows steady state crystallization by diffusion, is reported.

II. Experimental procedure:

2.1 Advantages of the VDS process

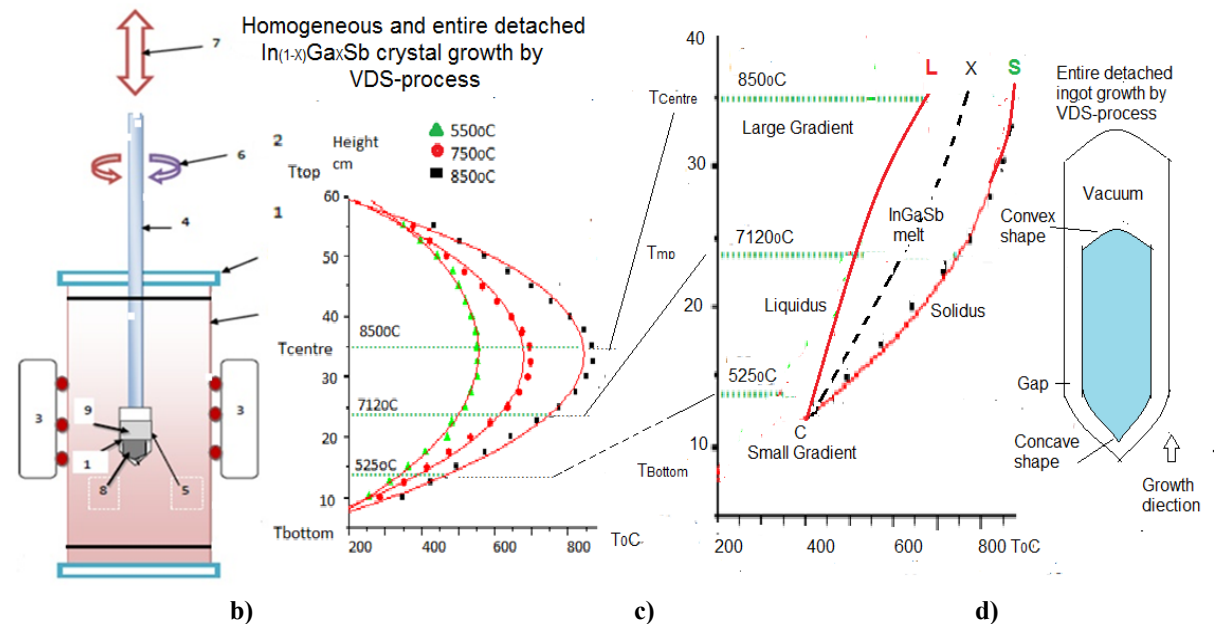


Figure- 1 a) The schematic diagram of VDS process. b) The temperature profile, the height of furnace was 66cm, and the hot zone of furnace was at 850°C at the centre (33cm) the axial temperature gradients were increasing from the bottom of furnace towards centre T_{centre} (850°C). c) The enlargement of fig1-b is showing the separation of melt and crystal phases. In_{0.5}Ga_{0.5}Sb growth process, the small gradient of melt (12°C/cm) was the freezing point at m.p. 525°C of InSb, then, as a length of entire detached crystal increases with the upward moving meniscus and crystal-melt interface into the increasing temperature gradient up to the larger gradient (28°C/cm) at m.p. 712°C of GaSb. This was the phase transformation of molten melt phase to steady state crystallization phase, which was grown by the entire detached or contactless growth mechanism into vacuum sealed ampoule into VDS process, where, conventions were suppressed due to the medium analogues to microgravity. d) Schematic as grown entire detached or contactless ingot (light blue colour) with a gap of the inner ampoule wall and as grown ingot. Interface shape seen from a top of melt into ampoule – initially a concave, middle flat, at the end convex, then, above it a vacuum.

The controlled VDS configurations, Sbbased bulk entire detached crystal was grown experimentally. Growth was encompassing the constant heat rate, the steady thermal field, the increased thermal gradient in single zone fixed vertical furnace, and a rotating ampoule. Then, the different axial temperature gradients and the cooling rates were designed and fabricated for a non-linear axial temperature gradient, and non-equilibrium thermodynamic medium into a vacuum sealed ampoule. The growth process was consists of the precise vertical furnace temperature profile, the axisymmetric constant heat, and the growth chamber as a thermal seal to surrounding. The constant heat, thermal field and increased vertical axial temperature gradient was played a dominant role in an isotropic vacuum sealed solute solution into ampoule. The enhanced crystallization by an entire detached growth was grown due to heat and mass transfer by diffusion into controlled VDS configurations.

2.2 The ampoule translation velocity

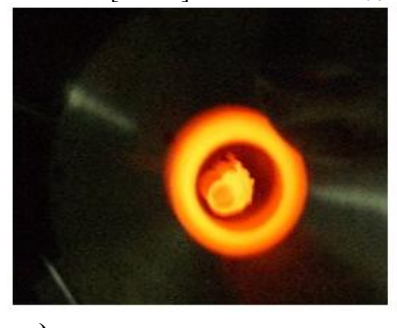
The controlled VDS configuration, the non-linear temperature gradient profile of the vertical furnace, the low $dT/dZ=12^{0}$ C/cm to high $dT/dZ=21^{0}$ C/cm were selected for $In_{0.5}Ga_{0.5}Sb$ growth from Fig-1. Thus, the controlled heat and mass transfer by

diffusion at crystal-melt interface front for melt velocities equation in [35-38, 64] were used for calculation of the translation velocity 'v' < 9cm/h to suppress the thermal and solutal convections into melt to grow the steady state crystallization. The thermal conductivity or the thermal diffusivity of the quartz ampoule wall is $\sim 0.01 \text{cm}^2/\text{s}$, hence, for Sb-based materials the solidification velocity was chosen $\sim 1/10^\text{th}$ of 'v'. The translation velocity selected 'v' < 9mm/h. The seventy-two entire detached Sb-based crystals were grown by the translation velocity rate <5mm/h [42-71] since 1994. In_{0.5}Ga_{0.5}Sb growths,

the solidification or freezing rate 'v' was selected ≤ 3 mm/h.

2.3 The vacuum sealed ampoule

In VDS experiments, the quartz tube as the growth chamber having 10cm diameter and 100cm length, and a quartz ampoule with a diameter 12-18mm, length 100mm, and cone angel (~45°to~75°) were used. The source materials of high-purity In, Ga, Sb (5N, Alfa Aesar) were taken in stoichiometric proportion into an ampoule. The oxygen,







a)

Figure-2 the photographs of different thermal intensities of molten In_{0.5}Ga_{0.5}Sb inside an ampoule (inner ring) and into the growth chamber (outer ring) for differ hot places during growth at constant cooling rate 0.0012°C/s, see Fig-1, a) at T_{centre}, the highest gradient 32°C/cm at T=850°C, the furnace height was 33cm, b) at T_{mp}, the gradient 22°C/cm at T=700°C, the furnace height was 17cm, c) T=T_{bottom}, the gradient 12°C/cm at 525°C (m.p. of InSb), the furnace height was 13cm for In_{0.5}Ga_{0.5}Sb melt was transformed from the melt phase into the solid phase by the transformation.

h)

and impurities contamination were prevented by purging high-purity inert argon gas in an ampoule having vacuum (~1.3x10⁻³ Pa), and an ampoule was back refilled alternately for 10 times. Ampoule was positioned vertically in an exclusive prearrangement in a vertical growth furnace to avoid the gravitational directional effects. Growths were performed - a) the vacuum sealed and the source materials into an ampoule and no back filling argon gas, and b) the back filling an argon gas (0.027-0.041MPa) and the source materials into an ampoule, but results were similar in both growths.

2.4 The In_{0.5}Ga_{0.5}Sb growth by the controlled VDS configuration

In_{0.5}Ga_{0.5}Sb growth, the vacuum sealed ampoule with the source materials was positioned vertically in a vertical single zone stable furnace of a non-linear temperature profile ($T_{centre} > T_{mp} > T_{bottom}$) Fig-1. The seven steps comprehensive temperature profile was applied –

c)

- I) The furnace temperature was reached to 850°C within 3h by a constant heat (220V, 10A), then, an ampoule kept at the temperature gradient 32°C/cm and a cooling rate 0.08°C/s for 12h to acquire concentration and density distribution into solute solution. Further, an ampoule was rotated (10rpm) till end of growth to stir a melt for homogeneous and congruent composition.
- II) An ampoule was translated downward with a lowering velocity rate 10mm/h to reach 50°C above the melting point of GaSb (765°C) within 5h, here, the temperature gradient was 32°C/cm, a cooling rate 0.005°C/s, then, kept 7h for the chemically uniform thermo-solutal solution.
- III) In the hot zone at $T_{mp}>T_{bottom}$, ampoule was ascertained to move from 712°C to 525°C or the vertical gradient range 21° C/cm to 12°C/cm.

IV) The principle of In_{0.5}Ga_{0.5}Sb detached growth process: The In_{0.5}Ga_{0.5}Sb solidification was processed in increasing axial thermal gradient, keeping the constant heat rate at fixed furnace. Then, the melt was translated downward 3mm/h for unidirectional solidification at set temperature 765°C from a vertical furnace of height 28cm with a slow freezing rate or a steady cooling rate 0.0012°C/s. The axial temperature gradients range was larger 28°C/cm at furnace height 27cm, and smaller 12°C/cm at furnace height 13cm along axis. The freezing point of growth was increasing with an axial temperature gradient from 12°C/cm to 28°C/cm Fig-1. Growth starts at the low gradient freezing point (12°C/cm) at 'C' for InSb (525°C), then, a freezing point gradient increasing (28°C/cm) towards GaSb freezing point

 (712^{0}C) with the increasing length of solidification along axis during growth, Fig-1, 4 [2]. The radial gradient was low and constant at 1.4^{0}C/cm . In_{0.5}Ga_{0.5}Sb solidification growth time was 53h for 14cm, including the length of ingot. Ingot length was 6cm, and growth time was 24h, then, the crystal growth rate was v=1/t=2.5mm/h.

V) The ingot was lowered below 100°C m.p. of InSb with a cooling rate 0.01°C/s by an ampoule translation 10mm/h in 3h, and kept at 425°C for 12h for thermal stabilization. VI) Set temperature 765°C lowered to 250°C in 3h with a cooling rate 0.05°C/s to reduce the thermal stress in the grown ingot.

VII) Finally, the furnace supply was switched-off, then, In_{0.5}Ga_{0.5}Sb solidified ingot was taken out from

furnace, after 2h, Fig-3, and the polished ingot is in Fig-3d [6-15].

Gross solidification growth time was ~99h. The heat of conduction was prevented as no downward support to ampoule. The VDS configuration was controlled by PID controller. The substrate of $500\mu m$ thick cut transverse and longitudinal from as grown ingots, the samples dimensions were 10mm x 10mm x 0.3mm, then, these were lapped and polished [42-48, 51-60]. In_{0.5}Ga_{0.5}Sb, XRD showed that all the entire detached growths having the preferential crystallization direction (220) and reflection showed (110) orientation, and the blue shift was towards

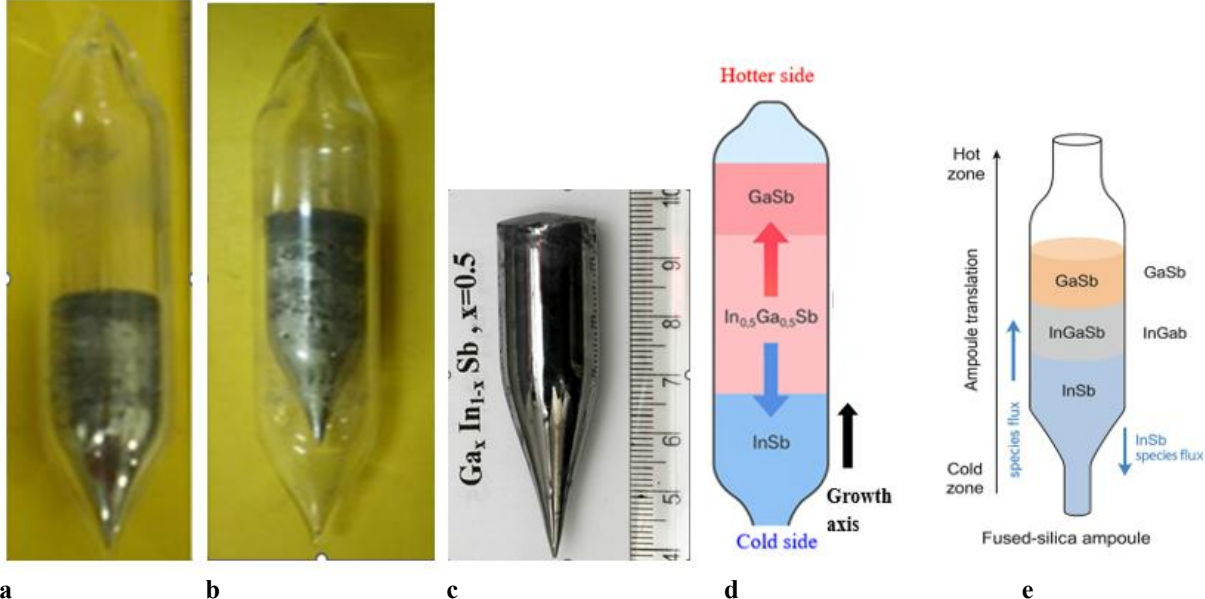


Figure-3 Detached or contactless In_{0.5}Ga_{0.5}Sb ingots, a) the ingot grown into a conical section of ampoule, b) the detached ingot moving away from a conical section of ampoule, c) another ingot's detached movements inside the ampoule, d) as grown ingot after chemical washing, cleanning and polishing. e) The first to freez solid showed the concave interface, while the last grown solid showed the convex interface shape (seen from the top of melt)

the lower incident angles, and FWHM < 112arcsec. These reveals the enhanced crystallization by an entire detached growth [56, 65-67]. The equipment used for characterization are listed in [67] for the thermal field and

phase transformation Fig-2, the detached growth Fig-3, the composition distribution Fig-4, and the growth of uniform boundaries in Fig-5, 6 are reported in this article.

The investigations of In_{0.5}Ga_{0.5}Sb growth -Firstly, all ingots were entirely detached or contactless. All ingots came out by smooth taping, and the ingot diameter was smaller than the inner diameter of an ampoule; ingots were shining in conical section, and was dull in cylindrical surface, while no micro bands on ingot surfaces. All ingots were free from striations; hence, it showed the higher crystallization by detached growth [21-22]. In steady state solidification, the surface roughness was similar to the detached growth in space (microgravity) [6-15]. The voids on ingot surface were the gas bubbles due to the local thermal stress on ingot surface during cooling process, [21-22]. The investigation showed the increased axial temperature gradients (12- 28° C/cm), the steady state cooling rate (0.0012°C/s) and translation velocity (10mm/h). The increased gradients were inhibited all convections [6-9] at equilibrium, hence, the solute accumulation near interface was increased due to non-existence of convections. The detached crystal growth rate was

2.5mm/h, which was larger than InGaSb grown in space (0.16mm/h), on Earth (0.11 mm/h) [27-34], and by VGF on Earth (0.12 mm/h) [33]. It showed changes in the concentrations and temperatures of the crystal-melt interfaces, and leads to alter the extreme growth velocities to ensure the macroscopic stability. Perhaps, the detached crystal growth rate was atomic incorporation process of InSb and GaSb, hence, it was faster than the mass transport by convection or by diffusion, since, the transformation process of crystallization was by dominant diffusion under the controlled VDS configuration.

III. Results and discussions:3.1 Thermal field and phase transformation

In controlled VDS configuration, comprehend steady state thermal field and phase transformation of In_{0.5}Ga_{0.5}Sb growth, it was experimentally studied. The three conditions of temperatures were investigated form Fig-1 - i) at T>T_{mp}, it exceeds the free energy of molten state at melting temperature. ii) at T<T_m, the free energy of the crystallization state was lowest. iii) at T=T_m, the melt free energies and the crystallization state at equilibrium, and was an ideal condition for the phase transformation of the melt phase to the solid crystalline phase [16-19, 31-38]. Therefore, Wilson seal at the bottom of growth chamber was removed to take photograph of the thermal images at six different hot places along growth axis by placing a mirror below the bottom of growth

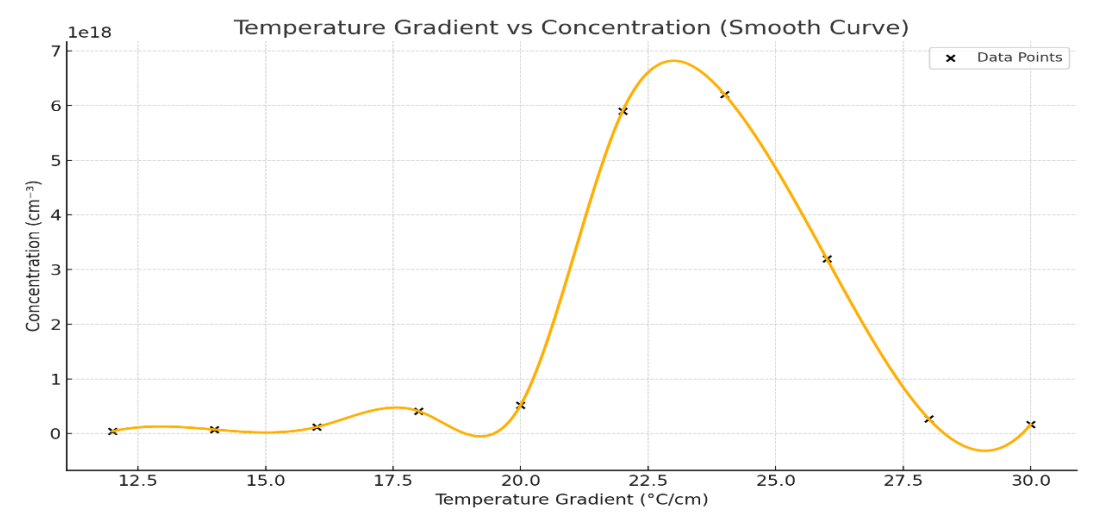


Figure- 6 The temperature gradient against the concentration of ingot along the ingot length

chamber in Fig-1 [63]. Also, the melt temperatures were measured with an enclosed thermocouple along the ampoule walls. The comprehensive steps were

- I) First thermal image in Fig-2a at T_{centre} , the highest gradient the equal temperature intensities at equilibrium thermal field.
- II) Second thermal image in Fig-2-b, below T_{centre}, the gradient was 28°C/cm at 765°C, and a furnace height was 27cm. The translation velocity was 10mm/h 32°C/cm at T=850°C and furnace height was 33cm and the constant cooling rate 0.0012°C/s. The growth chamber (outer larger ring) and In_{0.5}Ga_{0.5}Sb thermo-solute solution into ampoule (inner ring), the both rings were having throughout growth. However, the outer ring temperature intensity or thermal field state was as in step 'I', but an inner ring temperature intensity of melt was slightly reduced.
- III) Third thermal image in Fig-2c at T_{mp}, the gradient was 22°C/cm at T=700°C, and the furnace height was 17cm. The outer ring temperature intensity or thermal field state was as in step 'I', but an inner ring temperature intensity of melt was further slightly reduced.

- **IV)** Fourth image in Fig-2d at above $T=T_{bottom}$, the gradient was 17.5° C/cm at $T=600^{\circ}$ C, and the furnace height was 15cm. The outer ring temperature intensity or thermal field state was as in step 'I', but an inner ring temperature intensity of melt was further slightly reduced.
- V) Fifth thermal image Fig-2e, T=T_{bottom}, the gradient was 12°C/cm at 525°C (m.p. of InSb), and the furnace height was 13cm. Growth was advanced upward direction till the highest gradient 28°C/cm at 712°C (m.p. of GaSb), and the furnace height was 27cm. The outer ring temperature intensity of thermal field was as in step '1', but an inner ring temperature intensity of melt was transformed from a reddish spot to a darkish spot (solid).
- VI) Sixth thermal image Fig-2f at T<T_{bottom}, In_{0.5}Ga_{0.5}Sb melt was transformed from the melt phase into the solid phase by the slow transformation due to the slow decreasing thermal gradients. The small spherical darkish spot was grown as an oriented seed from a homogeneous nucleation by the reducing its volume, then the bulk crystalline solidification (an entire detached growth) phase was grown at crystal-

melt interface front. An increasing axial temperature gradient (1.2°C/mm) to (3.2°C/mm) and a cooling rate (0.0012°C/s) was investigated, and were compared with InGaSb crystal grown in space by

VGF [34], the temperature gradients 0.64 °C/mm (μ g) and 0.58 °C/mm (1g) in a space. Thus, solidification rate was faster in VDS process, because of entire detached growth due to dominant diffusion.

3.2 Growth mechanism in VDS process

I) The homogeneous and oriented self-seeding:

Comparison: Original ST (large units) vs Normalized ST* (dimensionless)

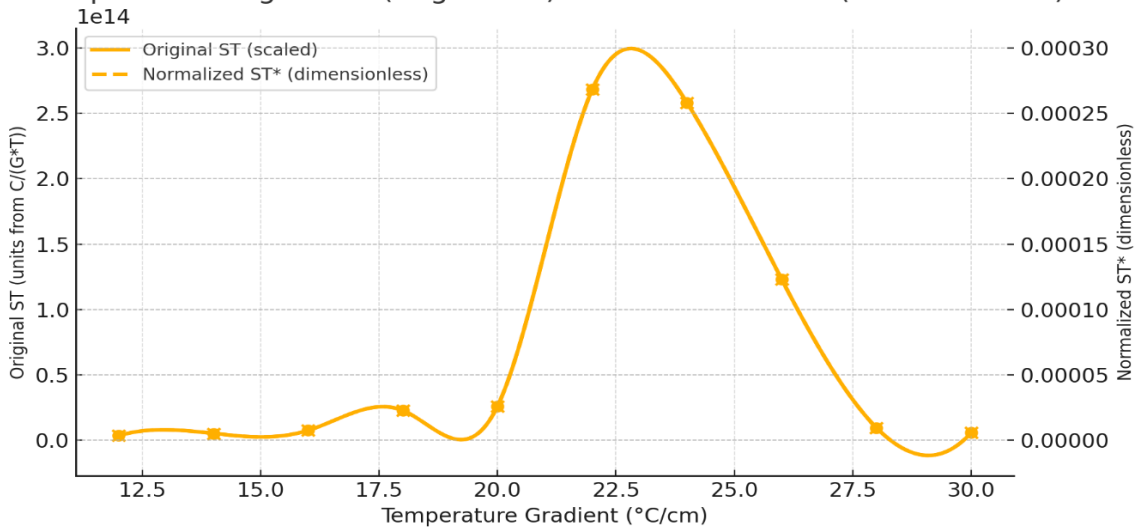


Figure-7 the temperature gradient versus Soret coefficient and normalized dimensionless Soret coefficient

Fig-2f, sect-3.1, a tiny spherical melt phase (darkish spot) of In_{0.5}Ga_{0.5}Sb solute solution hang at equilibrium state at T=T_m. Consequently, a blackish solid phase shrinks by a low temperature thermal gradient and low surface tension field force, and it freezes as a single homogeneous nucleation in a conical shape of ampoule, when, a melt cooled below its melting point. It was generated a gap between the circumference of ingot crystal phase and inner wall of an ampoule in continuous process as "the entire detached growth". Then, it grows an oriented solid phase by phase transformation at steady state thermal field [31-41] by heat and mass transfer due to dominant diffusion. Second principle was the classical approach; where, the crystalline fluctuations grow in the undercooled melt as small spherical drop of the bulk crystalline phase by a sharp crystal-melt interface from the droplet model or capillarity by the consequences of detachment. While, the kinetic energy of this approach relates the nucleation rate to the detachment rates of the molecules to form the crystallization [40]. Gap was articulated between the circumference of ingot and inner wall of an ampoule; thus, the curvature was interconnected between the inner wall of ampoule and on an oriented seed surface as a 'meniscus', while crystal-melt interface was established on seed surface. In VDS process, the solute accumulates first at centre and solute solution

was at periphery, hence, a crystal-melt interface and a meniscus were continued as "an entire detached growth" in upward growth direction till the melt get over. Ingot length was increased at the variation of meniscus and interface shape - initially concave, concave to flat, then flat to convex, and larger convexity at end (seen from a melt top). The measured variable gap width for different ingots was ranges $45\text{-}241\mu\text{m}$, and the height of interface was 0.5-2mm, Fig-3.

II) The three types of gaps ('d')

The contact angle (θ) and growth angle (α)were modified a meniscus shape and decide a gap width (d) at oriented seed position, then continually grows till an end of melt. Therefore, the three types of gaps ('d') using geometric concept of triple phase line (TPL) were investigated. In TPL frame, one vector was along a surface of alloys ingot, second was vector along an interface line, and third vector was along meniscus curvature [6-19, 21-22]. Then, the comprehensive three type of gaps were investigated - i) Gap width constant 'd': the TPL frame was no movement along a growth axis, then, phase vector frame was steady, thus, the gap width was constant (~115µm). ii) Gap width 'd' decreases: TPL frame was dynamic and movement was in the anti-clock wise along a growth axis inside a gap width, thus, the gap width was decreased (231-105 μ m) [50]. iii) Gap width 'd' increases: TPL phase frame was dynamic and movement in the clock wise along a growth axis and away from an ampoule wall into a melt, thus the gap width was increased (95-250 μ m) [57-58].

An entire detached growth by VDS process, the measured meniscus height (250 μ m) and the interface convexity (0.5 to 2mm) reveal weak convections by the controlled mass transport phenomenon [22, 30-34]. Gap width was 250 μ m in VDS against a gap

width of 350µm for crystals grown in a space [12-13], thus gravitational effect was no impact on a meniscus and interface [18, 19], because, locally at crystal-melt interface, the detached growth medium was fulfilled analogues to microgravity medium though into above melt, the gravity effect was present, thus, VDS is a very complex growth process. The three gap widths were investigated from dynamics of TPL frame - i) the constant, ii) the decreased, and iii) the increased [11-15, 21-22].

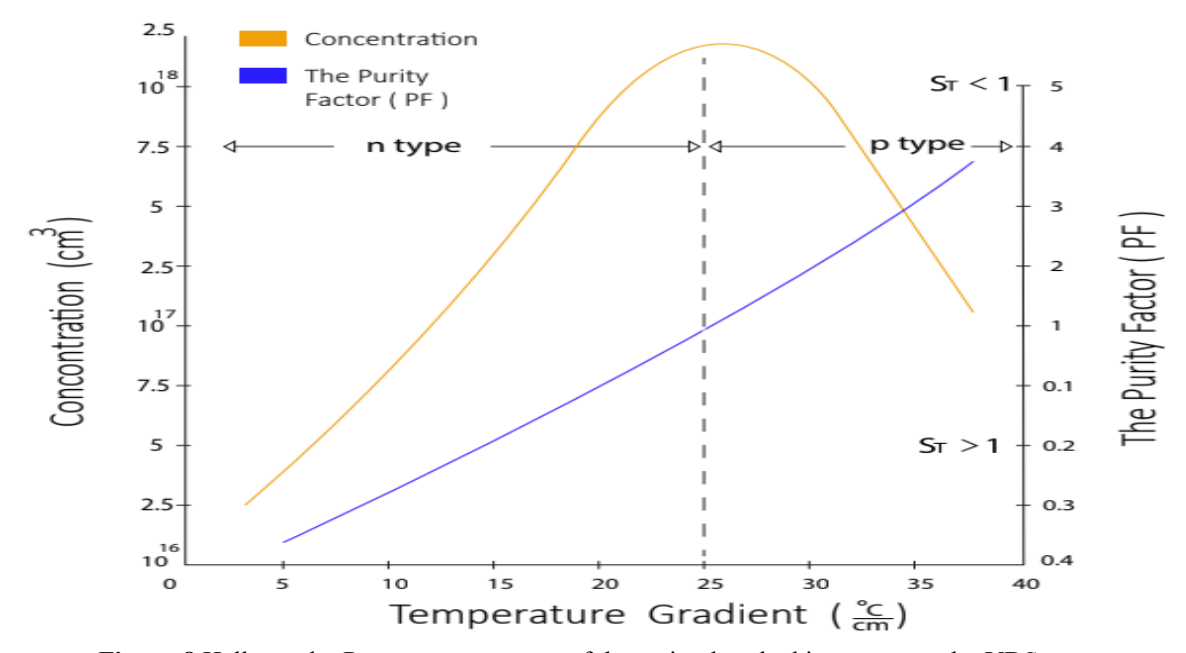


Figure-8 Hall-van der Pauw measurements of the entire detached ingots grown by VDS process

3.3 The enhanced crystallization by detached growth

In_{0.5}Ga_{0.5}Sb entire detached growth into VDS process, electro-physical measurements by Hall-van der Pauw are shown in different colours for parameters in Fig-4 - Red: Mobility (µ), decreased from 4.1×10^4 cm²/v.sec to 1.2×10^3 cm²/v.sec, Green: Carrier concentration (η) increased from (η) $2.5 \times 10^{16} \text{cm}^{-3}$ to $6.1 \times 10^{17} \text{cm}^{-3}$, Orange: Resistivity (p) decreased from $6.3 \times 10^{-3} \Omega$.cm to $3.2 \times 10^{-3} \text{cm}^{-3} \Omega$.cm, and Blue: Hall coefficient (Rh) decreased then again increased. The band gap engineering showed increasing from 0.19eV to 0.81eV [65-67]. In parameters variation, the In, Ga, and Sb atoms or InSb-GaSb phase comparative motion in a solute solution due to the heat distribution and increasing axial temperature gradient consists of composition phases by concentration gradient. Further, the solute was continuously accumulated at flat crystal-melt interface front, and was transformed to a solid phase with enhanced crystallization by an entire detached growth due to heat and mass transfer by the dominant diffusion. $In_{0.5}Ga_{0.5}Sb$ ingot length was divided in three regions in Fig-4a.

Region I: The substrates cut between 1%-45% of composition Fig-4b [2] showed the heavier 'InSb' binary constituent element was accumulated into the conical side (low gradient at 525°C). Then, the concentration gradient was established into In_{0.5}Ga_{0.5}Sb solute solution, InSb first freezes with the incorporation of 'GaSb'<0.1% in In-Sb chain (solute solution). Whereas, from Fig-4, [2] 'GaSb% composition increases from 0.1% to 45% with the composition range $In_{0.99}Ga_{0.01}Sb$ to $In_{0.55}Ga_{0.45}Sb$ along axis. In_{0.5}Ga_{0.5}Sb as a semiconductor, Rh and μ decreases smoothly, and $\boldsymbol{\eta}$ and $\boldsymbol{\rho}$ increases smoothly, because, InSb composition was decreasing with increasing composition of GaSb, and over all composition [65] was attributed to heat selfbalancing of In_{0.5}Ga_{0.5}Sb composition.

Region II: Middle ingot region, the substrates cut in between 45% to 55% of GaSb% composition. Interestingly, for a steady state condition, the composition displays fluctuation of n-type and p-type

semiconductor carriers as a race to convert n-type to p-type semiconductor, it was very sensitive due to carriers' compensations. The composition ranges from $In_{0.55}Ga_{0.45}Sb$ to $Ga_{0.55}In_{0.45}Sb$ Fig-4. [2]. All parameters (Rh, μ , η , and ρ) were in race [65].

Region III: The lighter 'GaSb' binary constituent element was moved towards higher temperature, and accumulated into the top side of an ampoule (higher gradient at 712°C). The substrates cut from 55% to 99% of GaSb%, the composition range Ga_{0.55}In_{0.45}Sb

to $Ga_{0.99}In_{0.01}Sb$ was due to increased GaSb% composition, which was moved towards GaSb binary composition phase at end side Fig-4 [2]. In this range, the parameters η decreases and the μ , Rh and ρ increases smoothly [67], because, negligible small InSb% composition, while, GaSb% composition was in majority %, and over all composition by the heat self-balancing $In_{0.5}Ga_{0.5}Sb$ composition [65]. Charge carrier mobility was extremely enhanced due to the compensation of donors and acceptors. The n-type

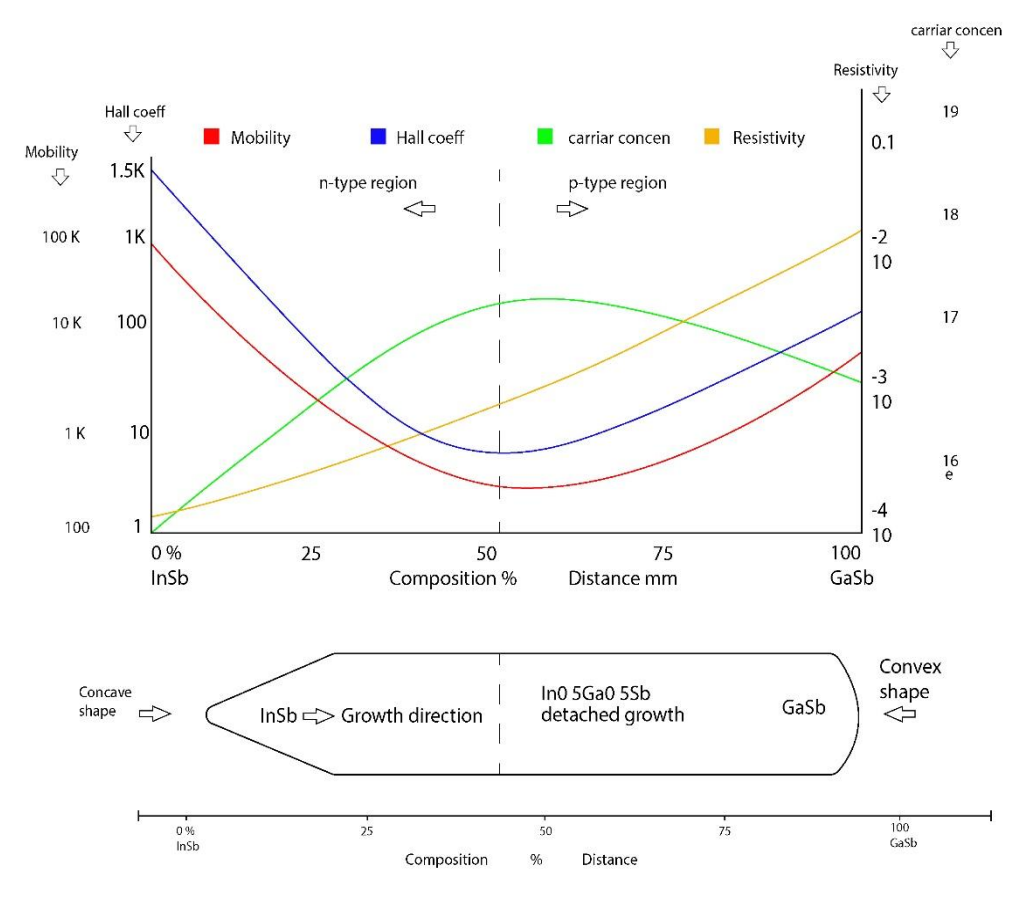


Figure-9 a) The composition analysis by the Hallvan der Pauw electro-physical measurements for the Mobility, Carrier concentration, Resistivity, and Hall coefficient of In_{0.5}Ga_{0.5}Sb ingot growth. (b) The schematic figure of as grown ingot. The ingot interface shape shown in a schematic diagram initially a concave shape, middle flat, at the end convex shape. Ingot is divided into three regions along the growth axis-i) Initially the InSb growth in the conical section (concave shape). ii) After conical section the middle region In_{0.5}Ga_{0.5}Sb ingot growth, iii) After In_{0.5}Ga_{0.5}Sb ingot growth at the end was GaSb growth as in Ref [2]. We envisage that paraphs it could be similar features of the thermal diffusion or Soret phenomenon as in reference [35-38]. Interface shape seen from a top of melt into ampoule - initially a concave (InSb), middle flat (In_{0.5}Ga_{0.5}Sb), at the end

convex (GaSb) into the vacuum sealed ampoule. The enhanced parameters variations reveal the heat and mass transfer by the dominant diffusion into the controlled VDS process, where, convections are annihilated due to a medium comparable to microgravity.

conductivity was for the higher InSb% composition, and p-type conductivity was for the higher GaSb% composition. Concentration changes of donor to acceptor were sensitive for compensation as heat and mass transfer by dominant diffusion (self-purification) [25], and heat (self-balancing) [35]. In VDS process, the temperature field was generated a concentration gradient into the solute solution of ternary melt, then at crystal-melt interface the mass flux of mass transfer was due to heat and mass transfer by dominant diffusion, then grow an entire

detached growth. In_{0.5}Ga_{0.5}Sb growth, the temperatures of solidification phase (concentration phase) were underneath the temperature of thermosolutal solution phase (melt composition phase) during steady growth process. From Fig-4, the heavier atoms of InSb concentration were moved to the low gradient side, while, the lighter atoms of GaSb concentration were moved to the higher gradient side. Thus, InSb% concentration composition was gradually decreased, and the GaSb% composition was gradually increased in an upward growth direction along axis against gravity vector in Fig-1c. This composition variations were according to the increased axial temperature gradients InSb-GaSb binary phase diagram in Ref. [2]. Hence, in dominant diffusion, the changes in temperature with respect to time and space by the heat transfer into growth process related to the rate of temperature change to the distribution of temperature and grown crystal properties. In cooling of solidified crystal, the self-heat balanced solute solution composition rapidly solidified as growth time increased. Because, the meniscus and interface were moved towards the higher temperature gradient leading to gradual increase in growth temperature. Hence, the concentration gradient is advanced by the driving force of temperature gradient to reach the steady state condition. Because of the entire detached growth by VDS process by connectionless condition, which was analogues to microgravity medium. Then, the thermal diffusion or Soret phenomenon was in isotropic fluid system of an enclosed medium with no external forces, concentration gradient builds up due









Figure-10 the 2D preferential growth morphology depicts the phase transformation micro growth in an entire detached ingot, a) the substrate photograph from left peripheral section of ingot showing the melt flow feature away from periphery of substrate, b) the substrate photograph from right peripheral section showed the steady state crystallization phase, wherein, the uniform growth or without micro growth was transpired due to the steady state thermo-solute velocity flow across the steady state interface front, c) the substrate photograph from centre of ingot showed excessive unreacted antimony (Sb) grown as a eutectic phase by transformations of solid-state phase at equilibrium, d) the substrate photograph from central part of ingot is similar as in Fig-b. the driving force of temperature gradient until the steady state condition reach, and the convections were neglected due to microgravity [35-38].

3.4 The micro growth and uniform boundaries

The micro-uniform growth and uniform boundaries in In_{0.5}Ga_{0.5}Sb growth were associated with a flat interface front and the solidification phase due to the momentum of melt phase by the heat and mass transfer by dominant thermal diffusion, as depicted in Fig-5, 6. The thermal field force in Fig-5a was forced the peripheral thermo-solutal velocity

flow (melt) away from periphery towards a centre. Here, the native interfacial velocity was driving force at flat crystal-melt interface, and local interfacial momentum of melt phase flow as the momentum of the dynamic velocity flow grown as the kinetic energy force, which was confined as a thermal stress at periphery on steady state crystallization. Whereas, the dislocation free growths in Fig-5b, d were the steady state crystallization phase, wherein, the uniform growth or without micro growth was transpired due to the steady state thermo-solute velocity flow across the steady state interface front accumulate sulute-solution, either in longitudinal or transverse direction, hence no thermal stress. Then, the stable momentum converted the smooth phase transitions from melt phase to steady state crystallization phase [31, 37-39]. The two uniform straight blackish lines in Fig-5c were excessive unreacted antimony (Sb) grown as a eutectic phase by transformations of solid-state phase at equilibrium. In second example of micro growth into entire detached growths are shown Fig-6.

The uniform boundary in fig-6a, the steady state crystallization was grown by the two transformations (dark and light), and free from slip bands during crystal cooling. The oriented rightangled solid-state phase growth of 'Sb' (dark) in Fig6b was the ordered phase transformation on $In_{0.5}Ga_{0.5}Sb$ parent phase (light) at stationary interface front. The oriented right-angled step by step growth in Fig-6c was solid-state phase of 'Sb' (dark) on $In_{0.5}Ga_{0.5}Sb$ parent phase (light). The two phases in Fig-6d grown $In_{0.5}Ga_{0.5}Sb$ crystalline phase (light) and solid-state phase of 'Sb' (dark) [37-38].

The diffusion driven transportation process into VDS process, the interface front local melting temperature was slightly deviate from the factual interface temperature, and grow as a slip into solidification phase due to crystal growth velocity at flat crystal-melt interface [35-36]. In thermal stress-

free growth, the reduced dislocation density by an entire detached growth was $1.42 \times 10^3 \text{cm}^{-2}$ to $5.29 \times 10^3 \text{cm}^{-2}$ by. It was compared with dislocation density of InGaSb crystal [34] grown under µg $2.16 \times 10^4/\text{cm}^2$ and under 1g $2.72 \times 10^4/\text{cm}^2$. However, the detached growth by VDS process, the local momentum perturbation at interface front grows uniform boundaries, and the 2D thermal effect across the section of ampoule at two phases of alloy and the flat crystal-melt interface, where, the momentum of heat and mass transfer by thermal diffusion was grown the local boundaries into steady state crystallization.

IV. Conclusion:

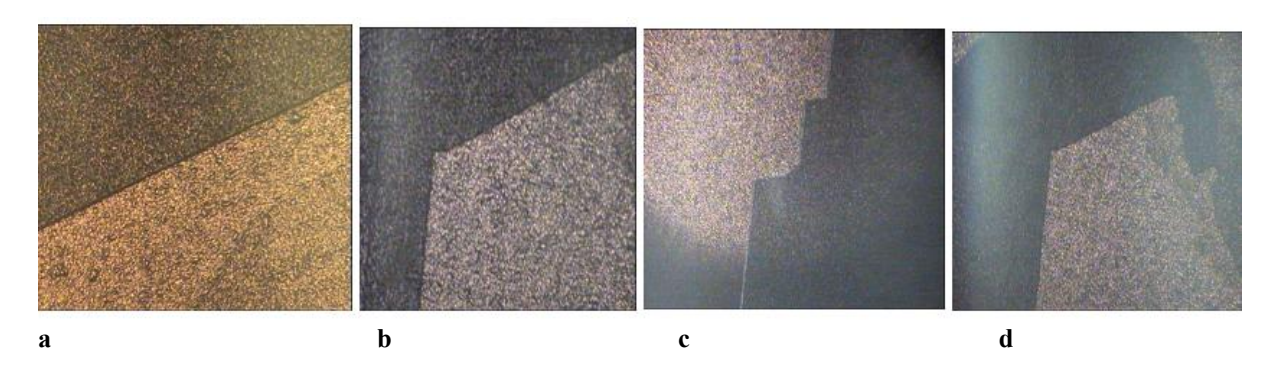


Figure-11 the 2D preferential growth morphology depicts the phase transformation, the parent phase of the crystalline In_{0.5}Ga_{0.5}Sb phase or parent phase (light) and the solid-state phase (dark) a) the periodic 2D crystal geometry for two crystals phases (dark and light) separated by thin dislocation line regions and having a common tilt axis oriented along the z-axis. The two phases are in ordered fashion of atomic or molecular level by entire detached ingot crystal growth, b) the angular growth by the solid-state phase orientations growth (dark) on parent phase (light), c) the growth represents the step by step orientations growth of the solid-state phase (dark) while parent phase growth (light) is continuous, d) these two grown phases are one parent phase (light) of In_{0.5}Ga_{0.5}Sb growth phase, while the second dark oriented solid-state phase of excess unreacted antimony (Sb) grown as solid state phase. InSb atoms toward the colder zone and lighter GaSb atoms toward the hotter zone, balancing solute segregation and maintaining interface planarity.

First time, In_{0.5}Ga_{0.5}Sb growth by VDS process, A modified VDS process has been successfully developed for the growth of high-quality In_{0.5}Ga_{0.5}Sb crystals under fully detached conditions. The entire crystal–melt detachment, maintained by a fine vapor gap along the ampoule wall, eliminates wall-induced convection and lateral heat leakage, producing a diffusion-dominated growth regime.

The combined influence of thermo-diffusion (Soret effect) and quasi-equilibrium interface control replicates the solidification characteristics of microgravity on Earth. The positive Soret coefficient drives heavier The grown crystals exhibit: Excellent structural perfection, FWHM < 100 arcsec, Low dislocation density, < 10^3 cm $^{-2}$, Uniform composition, $\Delta x < 0.01$ across the crystal length, and enhanced electrical mobility, up to 2.5×10^4 cm 2 V $^{-1}$ s $^{-1}$. the increased crystal growth rate 2.5mm/h, and the enhanced crystallization by an entire detached growth were investigated.

The controlled heat rate, thermal field and axial gradient in VDS process was manifested an entire detached solidification by heat and mass transfer by dominant thermal diffusion. The thermal diffusion was depended on the concentration gradient and the increased axial temperature gradients. For successful entire detached growth, the composition solidification point must below isotherm of a meniscus position, and the flat crystal-melt interface, and a stationary isotherm perpendicular to a growth axis. The thermal diffusion controlled VDS experiment is a key to evaluate a new scientific vision of physics at equilibrium. Detached growth is a new research field diminishing trial-and-error investigation of physics-based simulations.

References:

- [1] T J Bright, Liping Wang, Z M Zhang, J heat transfer 136 (2014) 062701
- [2] G. B. Stringfellow, Phys. Chem. Solids 33 (1972)
- [3] W.R. Wilcox, J.F. Yee, M.C. Lin, K. Sarma, S. Sen, InSb–GaSb alloys, in: G.W. Morganthaler, G.E. Simonson (Eds.), Skylab Space Exp, American Astronaut Society, Tarzana, 1975, 27
- [4] A.F. Witt, H.C. Gatos, M.C. Lavine, C.J. Herman, J Electrochemical Society 122 (1975) 276
- [5] J.T. Yue, F.W. Voltmer, Journal of Crystal Growth 29 (1975) 329
- [6] Wilcox, W. R.; Regel, L. L. Microgravity Sci. Technol. 8 (1995) 56, abid, 14 (1999) 166
- [7] Yazhen Wang, Liya L. Regel, William R. Wilcox J Crystal Growth 209 (2000) 175
- [8] Yazhen Wang1, Liya L. Regel, William R. Wilcox J Crystal Growth 243 (2002) 546
- [9] Wang, J. B.; Regel, L. L.; Wilcox, W. R. Journal of Crystal Growth 260 (2004) 590
- [10] Duffer, T.; Paret-Harter, I.; Dusserre, P. J. Crystal Growth 100 (1990) 171
- [11] T. Duffar, P. Dusserre, F. Picca, S. Lacroix, N. Giacometti, J Crystal Growth 211 (2000) 434
- [12] T. Duffar, P. Dusserre, N. Giacometti, J Crystal Growth 223 (2001) 69
- [13] M. Fiederle, T. Duffar, V. Babentsov, K. W. Benz, P. Dusserre, V. Corregidor, E. Dieguez, P. Delaye, G. Roosen, V. Chevrier, and J. C. Launay, Cryst. Res. Technol. 39, (2004) 481
- [14] St. Balinta, L. Braescua, L. Syllab, S. Epurea,b, T. Duffar, J CrysGrowth 310 (2008) 1564
- [15] L. Sylla, J.P. Paulin, G. Vian, C. Garnier, T. Duffar, Materi Science and Eng A 495 (2008) 208
- [16] Carmen Stelian, Andrew Yeckel, Jeffrey J. Derby, J Crystal Growth 311 (2009) 2572
- [17] Andrew Yeckel, Jeffrey J. Derby, J Crystal Growth 314 (2011) 310
- [18] Andrew Yeckel, Prodromos Daoutidis, Jeffrey J. Derby, J Crystal Growth 356 (2012) 33
- [19] Andrew Yeckeln, Prodromos Daoutidis, Jeffrey J. Derby, J Crystal Growth 361 (2012) 16
- [20] Andres J. Gozaa, Stephanie E. Tritchlera, , Brent C. Houchensa, , J Crys Growth, 337 (2011) 60
- [21] A.E. Voloshin, A.A. Lomov, T. Nishinaga, P.Ge, C. Huo, J Crystal Growth 236 (2002) 501
- [22] A.E. Voloshin, T. Nishinaga, P.Ge, C. Huo, J Crystal Growth 234 (2002) 12
- [23] Kaoruho Sakata, Midori Mukai, Govindasamy Rajesh, Mukannan Arivanandhan, Yuko Inatomi, Takehiko Ishikawa, Yasuhiro Hayakawa, Advances in Space Research 53 (2014) 689
- [24] Jianding Yu, Yuko Inatomi, Velu Nirmal Kumar, Y. Hayakawa, Yasunori Okano, Mukannan

- Arivanandhan, Yoshimi Momose, Yan Liu, X. Zhang, Xinghong Luo, npj Microgravity 5 (2019) 8 [25] V. I. Strelov, I. P. Kuranova, B. G. Zakharov, A. E. Voloshin, Crystallog Reports, 59 (2014) 781
- [26] Yu. A. Serebryakova, V. N. Vlasova, V. S. Sidorova, I. A. Prokhorova, I. L. Shul'pinab, and E. N. Korobeinikovaa, J Surface Invest, Synchrotron and Neutron Techniques, Vol. 6 (2012) 604
- [27] Xin Jin, Bing Wang, J Cryst Growth 607 (2023) 127110
- [28] Nathalie Bergeon, G. Reinhart, Fatima L. Mota, H. Nguyen, Flowing Matter 44 (2021) 98
- [29] Masahiro N. Youhei Takagi, Yasuhiro Hayakawa, Sadik Dost, J Cryst Growth 385 (2014) 66
- [30] Xin Jin, Bing Wang, J Crystal Growth 607 (2023) 127110[31]
- Rachid Ghritli, Yasunori Okano, Yuko Inatomi, Sa dik Dost, J Crystal Growth 573 (2021) 126280
- [32] Rachid Ghritli, Yasunori Okano, Yuko Inatomi, Sadik Dost, Japan J Appl Phys 61 (2022) 115502
- [33] Rachid Ghritli, Yasunori Okano, Yuko Inatomi, S. Dost, J Chemi Eng Japan 56 (2023) 2222757
- [34] Yasuhuro Hayakawa, Mukannan A rivanadhan, Tadanobu Koyama, Yoshimi Momose, Kaoruho Sakata, Tetsuo Ozawa, Yuko Inatomi, Int. J. Microgravity Sci. Appl., 34 (2017) 340111
- [35] Peter Rudolph, AIP Conference Proceedings 1270 (2010) 107.
- [36] P. Rudolph, M. Czupalla and B. Lux, J. Crystal Growth 311, (2009) 4543
- [37] M.A. Rahman, M.Z. Saghir Interna J Heat and Mass Transfer 73, (2014) 693
- [38] Pierre Costesèque, Mojtabi Abdelkader, Jean Karl Platten, Thermo-diffusion phenomena. 339 (2011) 275-279 -
- [39] S. Akamatsu, S. Bottin-Rousseau, V. T. Witusiewicz, N. Bergeon, F. L. Mota, U. Hecht, M. Plapp, A. Ludwig, J. Mogeritsch, , G. Zimmermann, McFadden, W. Sillekens, npj Microgravity 9 (2023) 83
- [40] László Gránásya, Gyula I. Tóth, James A. Warren, Frigyes Podmaniczky, György Tegze, László Rátkai, Tamás Pusztai, Progrs Mater Sci. 106 (2019) 100569
- [41] Kaveh Dargahi Noubary, Michael Kellner and Britta Nestler, Materials 15 (2022) 1160.
- [42] D.B. Gadkari, Lal K. B., Arora B. M., Proc. DAE Solid State Physics Symp India, Vol. 37 C, (1994) 198, abid Vol. 38C, (1995) 198
- [43] D.B. Gadkari, Lal, K. B., Arora B. M., (Rapid Communication) J. Crys Growth 175 (1997) 585
- [44] D.B. Gadkari, Lal K. B., Arora B. M., Bull. Mater. Sci. 21 (1998) 127.
- [45] Gadkari D. B., Lal K. B., Arora, B. M., Indian Patent 139/BOM/1999 (1999) and 192132 (2004)

- [46] D.B. Gadkari, Lal K. B., Arora B. M., Indian J Pure Applied Phys 37 (1999) 652
- [47] D.B. Gadkari, Arora B. M., Indian J Pure & Applied Physics Vol. 38, (2000) 237
- [48] D.B. Gadkari, Lal K. B., Arora B. M., Bull. Mater. Sci. 24 (2001) 475
- [50] D.B. Gadkari, Proc. NSGDSC-2009, MRSI-Mumbai Chap India, November 19-21 (2009) 42
- [51] D.B.Gadkari, Arora B. M., Transaction Materials Soc Japan 34(2009) 571
- [52] D.B. Gadkari, J Chemi Chemi Enginee 6 (2012) 65
- [53] D.B. Gadkari, J Chemi Chemi Enginee 6 (2012) 250
- [54]. Gadkari Dattatray, J Materi Sci Engin A2, 9 (2012) 593
- [55] D. B. Gadkari, AIP Conf. Proc. 1512 (2013) 856
- [56] D.B. Gadkari, J Materi Sci Engineeg A3, 5 (2013) 338
- [57]. D.B. Gadkari, B.M. Arora, Mate Chemi Phys 139 (2013) 375
- [58]. D.B.Gadkari, Interna J. Sci Res Publ 4 (2014) 01
- [59]. Dattatray Gadkari, Intern J Enginee Appl Sci (IJEAS) 2 (2015) 39
- [60] Dattatray Gadkari, Dilip Maske, M. Deshpande, Brij Mohan Arora, IJIRSET 5 (2016) 20925
- [63] D. B. Gadkari, Int. J Engin Resea. Appli. 9 (2019) 01
- [64] D Maske, M Deshpande, D Gadkari, J Nano and Electroni Physics 12 (2020) 2012
- [65] D B Gadkari, Int J Eng Res App 10 (2020) 05
- [66] D B Gadkari, Int J Eng Res App 10 (2020) 35
- [67] D B Gadkari, Int J Eng Res App 10 (2020) 07
- [68] D S Maske, M Joshi, R Choudhary, and D B Gadkari, AIP conf. Proc. 1536 (2013) 876
- [69] M Deshpande, D Maske, B M Arora and D B Gadkari, AIP Conf. Proc. 1536 (2013) 333
- [70] Rashmi Choudhary, Dilip Maske, and Dattatray Gadkari, AIP Conf. Proc. 1536 (2013) 877
- [71] Manisha Deshpande, Dilip Maske, Devarani Devi, Rashmi Choudhari, BrijMohan Arora, Dattatray Gadkari, Inter J Sci Rese Pub, 5 (2015) 34